Journal of Molecular Structure 1294 (2023) 136385

Contents lists available at ScienceDirect

Journal of Molecular Structure

journal homepage: www.elsevier.com/locate/molstr

Achieving the cooperative and stepwise regulation of ESIDPT process in AFBD by introducing different electronic groups

Hongyan Mu [a,1], Dan Li [b,1], Jiaan Gao [a], Yang Wang [a], Yifu Zhang [a], Guangyong Jin [a,*], Hui Li [a,*]

[a] Jilin Key Laboratory of Solid-State Laser Technology and Application, School of Physics, Changchun University of Science and Technology, Changchun 130022, China
[b] State Key Laboratory of Luminescence and Applications, Changchun Institute of Optics, Fine Mechanics and Physics, Chinese Academy of Sciences, Changchun 130033, China

ARTICLE INFO

Keywords:
Dual intramolecular hydrogen bondings
Excited state intramolecular double proton transfer
Potential energy surface
Bonn-Oppenheimer molecular dynamics

ABSTRACT

In this paper, the effect of different electronic group substituents on the excited state intramolecular double proton transfer (ESIDPT) in AFBD is comprehensively researched by using quantum chemistry methods. Two electronic groups with comparable capabilities, including the electron-withdrawing group (-Br) and the electron-donating group (–OCH_3), are chose to accomplish this study. The obtained geometric parameters, reduced density gradient and infrared spectra calculations have demonstrated that AFBD and its two derivatives experience the ESIDPT process. Subsequently, the conclusion of the potential energy surface and Bonn-Oppenheimer molecular dynamics further unveil that AFBD undergoes a cooperative ESIDPT process at ~15 fs. Nevertheless, it should be noted that the introduction of -Br and –OCH_3 transforms the proton transfer path. That is: "the cooperative ESIDPT is converted into the stepwise ESIDPT". Besides, we also confirm that the substitution of the electronic groups OCH_3→H→Br can accelerate the ESIDPT process. Our work not only regulates the path of ESIDPT process, but also provides a time scale for this process, which is conducive to developing new intelligent fluorophores based on ESIDPT behavior.

1. Introduction

The excited state intramolecular proton transfer (ESIPT) process via intramolecular hydrogen bondings (IHBs) in organic compounds with bifunctional groups (acidic proton donor (-OH or -NH2) and basic proton receptor (−C═O or −C═N)) has long played a significant role in photophysics and photochemistry fields [1–3]. In general, dual fluorescence characteristics and large Stokes shift are the most representative signs of the ESIPT systems [4–9]. It is because of this tunable wide emission band that many molecules with ESIPT properties have been developed in a variety of scientific research fields such as fluorescent probes [10–12], molecular switches [13,14], organic luminous materials [15–17] and laser dyes [18].

In view of the previous reports, ESIPT has attracted a lot of attention and has been investigated through various experimental and theoretical methods [19–24]. For example, Li et al. demonstrated that the presence of the electron acceptor (-NO_2 group) in HBI molecule favored the ESIPT process, while the presence of the electron donor (-NH_2 group) hindered the ESIPT process [19]. Yang et al. revealed that nonpolar solvents are more beneficial to the ESIPT behavior of BDTBP compounds than polar solvents [20]. The attenuation of atomic electronegativity enhances the IHBs of URA and thus facilitating the ESIPT process, which has been proved by Shang et al. [21]. In other words, substituents, solvent polarity and atomic electronegativity can effectively adjust the ESIPT process. Particularly, the ESIPT also involves excited state intramolecular double proton transfer (ESIDPT). Recently, many scientific researchers have also successively explored the impact of external environment on the ESIDPT systems. Zhao et al. predominately probed into the ESIDPT process of HPBB compounds in aprotic solvents with different polarities [25], they proposed that polar solvents promote the stepwise ESIDPT process of HPBB. Yu et al. investigated the effect of solvents on the ESIDPT behavior in 7AI dimer [26]. They confirmed that the ESIDPT followed a cooperative mechanism in non-polar solvents and polar solvents with low dielectric constant. And in polar solvents with larger permittivity, the ESIDPT follows a stepwise mechanism. It can be seen that solvent polarity can effectively regulate the stepwise and cooperative mechanisms. The difference is that we have systematically modified the molecular structure through electronic groups with

* Corresponding authors.
E-mail addresses: jgycust@163.com (G. Jin), huili@cust.edu.cn (H. Li).
[1] Hongyan Mu and Dan Li contributed equally to this work.

https://doi.org/10.1016/j.molstruc.2023.136385
Received 16 June 2023; Received in revised form 22 July 2023; Accepted 8 August 2023
Available online 8 August 2023

Table 1
Indexes describing the ability of different electronic groups.

	AFBD–OCH_3	AFBD	AFBD-Br
electronic groups ggroups	OCH_3	H	Br
σp	−0.27	0.00	0.23

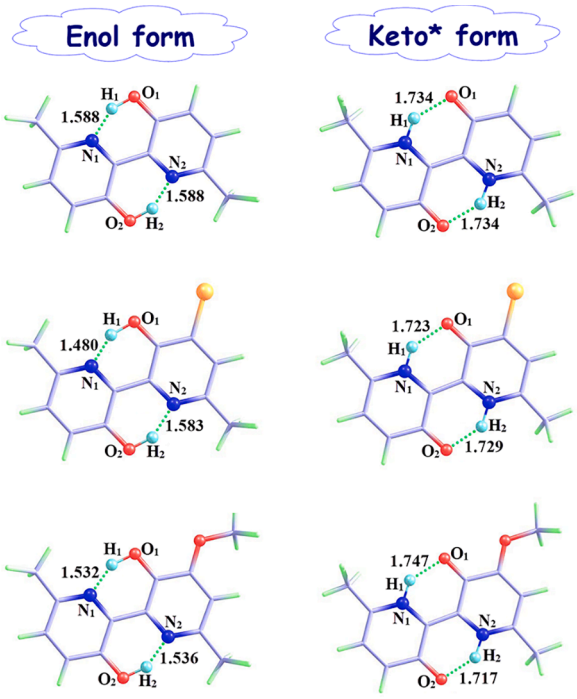

Fig. 1. The enol form in the S_0 state and the keto* form in the S_1 state of the AFBD (up), AFBD-Br (middle) and AFBD–OCH_3 (down).

different σp value (Table 1) and successfully realized the conversion of both mechanisms [27,28]. Wherein, the σp represents the ability of electron-withdrawing and electron-donating groups. The more negative the σp index is, the stronger the ability to electron-donating, the more positive the σp index is, the stronger the ability to electron-withdrawing.

The 4-Alkyne-Functionalized [2, 2′-Bipyridine]−3, 3′-diol (AFBD) is a typical proton transfer fluorophore [29]. Considering the pre-existing dual IHBs in the molecular structure, the ESIDPT process is likely to occur after photoexcitation. Therefore, based on density functional theory (DFT) and time-dependent DFT (TD-DFT) methods in this work, AFBD is used as an ideal model to explore the influence of different substituents on ESIDPT process. First of all, we optimize the geometric structure of target molecules and simulate the infrared spectra, which confirm the occurrence of ESIDPT process in AFBD and its two derivatives. Subsequently, the difference in charge distribution before and after electron transition are analyzed by frontier molecular orbitals and charge density difference maps. In addition, we perform relaxation scanning on the potential energy surface of S_0 and S_1 states, determining that the three compounds undergo the ESIDPT process in the S_1 state. Finally, we evaluate the characteristics of excited state hydrogen bonding dynamics under different substituents and reveal the path and time scale of the ESIDPT process.

2. Computational details

All calculations are performed using Gaussian software [30]. According to the theoretical research of Oftadeh et al., the reliability of 6–31++G basis set has been proved [31]. To further ensure the accuracy of the calculation, six different functionals with the 6–31++G basis set are chosen to calculate the absorption peak of AFBD and its two derivatives in acetonitrile solvent (see Table S1), and the result obtained by the B3PW91 functional is the closest to the experimental value. The geometric configurations of three compounds are optimized by the DFT and TD-DFT methods. Based on the optimized structure, we calculate the infrared (IR) spectra, frontier molecular orbitals (FMOs) and potential energy surface (PES) at the B3PW91/6–31++G theoretical level. Moreover, the IR spectra adopts a frequency correction factor of 0.972 [32–34]. With regard to the solvent effect of acetonitrile, it is considered to use the polarizable continuum model applying the integral equation formal variable (IEFPCM) in the calculation of self-consistent reaction field (SCRF) [35–37]. For the study of excited state hydrogen bonding dynamics in three compounds, the classical trajectory calculation (Bonn-Oppenheimer molecular dynamics (BOMD)) is implemented in the S1 state [38–40]. In addition, Multiwfn software [41] is used to analyze the reduced density gradient (RDG) and charge density difference (CDD) maps, and VMD software is used for visualization [42].

Table 2
The primary bond lengths (Å) of AFBD, AFBD-Br and AFBD–OCH_3 in the S_0 and S_1 states.

	AFBD		AFBD-Br		AFBD–OCH_3	
	S_0	S_1	S_0	S_1	S_0	S_1
N_1–H_1	1.558	1.037	1.480	1.036	1.532	1.034
H_1–O_1	1.049	1.734	1.076	1.723	1.057	1.747
N_2–H_2	1.558	1.037	1.583	1.037	1.536	1.037
H_2–O_2	1.049	1.734	1.042	1.729	1.056	1.717

3. Results and discussion

3.1. Structural analysis

Fig. 1 presents optimized geometric structures of the S_0 and S_1 states for AFBD and its two derivatives in acetonitrile solvent at the B3PW91/6–31++G level. It can be clearly observed that there are four intramolecular hydrogen bondings, which are named R_1 (O_1-H_1...N_1), R_2 (O_2-H_1...N_2), R_3 (N_1-H_1...O_1) and R_4 (N_2-H_2...O_2) respectively. In the meantime, Table 2 collect the primary structural parameters involved in the IHBs of three compounds in acetonitrile solvent.

As shown in Fig. 1, for the enol form, the R_1 and R_2 bond lengths of AFBD, AFBD-Br and AFBD–OCH_3 are 1.558 Å, 1.480 Å, 1.532 Å and 1.559 Å, 1.536 Å, 1.583 Å respectively. It is easy to see that the IHBs (R_1 and R_2) is strengthened under the substitution of electron withdrawing (-Br) groups. For the keto* form, we can observe that the original R_1 and R_2 have been broken and two new IHBs have been formed, namely R_3 and R_4. The R_3 and R_4 bond lengths in three compounds are 1.734 Å, 1.747 Å, 1.723 Å and 1.734 Å, 1.717 Å, 1.729 Å respectively. All the alterations demonstrate that the introduction of electronic groups can effectively affect the IHBs intensity, which is beneficial to the proceeding of ESIDPT in three compounds.

3.2. Reduced density gradient (RDG) analysis

The RDG function is first proposed by Yang and his co-authors [43], which can clearly describe the molecular interaction and the intensity of interaction in real space. As follows:

$$RDG(r) = \frac{1}{2(3\pi^2)^{1/3}} \frac{|\nabla\rho(r)|}{\rho(r)^{4/3}} \quad (1)$$

Wherein, $|\nabla\rho(r)|$ is the mode of electron density gradient, ρ(r) is the total electron density. Based on this, Lu and co-workers recently propose the interaction region indicator (IRI) isosurface [44], as shown in Eq. (2)

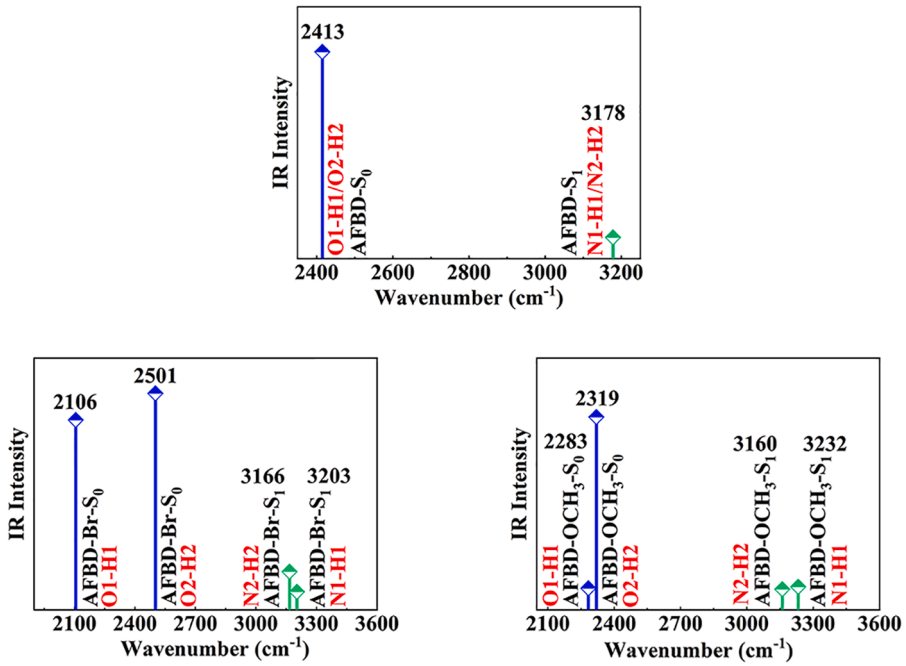

Fig. 2. The infrared (IR) spectra of AFBD, AFBD-Br and AFBD–OCH_3 in acetonitrile solvent.

$$IRI(r) = \frac{|\nabla\rho(r)|}{\rho(r)^a} \quad (2)$$

Herein, a is set equal to 1.1 in the standard definition. Same with the commonly used RDG analysis, the IRI isosurface can be used to distinguish diverse interaction intensity and corresponding characteristics in different regions simultaneously. The sign(I_2)r(a.u.) function in RDG is projected onto the IRI isosurface through different colors. The blue represents hydrogen bonding interaction, the red denotes steric effects and green refers to the Vander Waals (VDW) forces, respectively.

In order to reveal the position and intensity of intramolecular hydrogen bonding interaction, Fig. S1 provides the RDG diagrams and gradient isosurfaces of three compounds. The spikes in the circles indicate the strength of the intramolecular hydrogen bonding. In addition, the blue disks on the isosurface corresponds to the peaks in the circles.

In the S_0 state, the spike position at −0.07 ~ −0.08 for AFBD unveils the hydrogen bonding interactions of O_1-H_1…N_1 and O_2-H_2…N_2. The IHBs interactions corresponding to the AFBD-Br are O_1-H_1…N_1 and O_2-H_2…N_2 with the spike peaks of −0.09 ~ −0.10 and −0.07 ~ −0.08. There are two spike peaks with similar intensity near −0.08 in

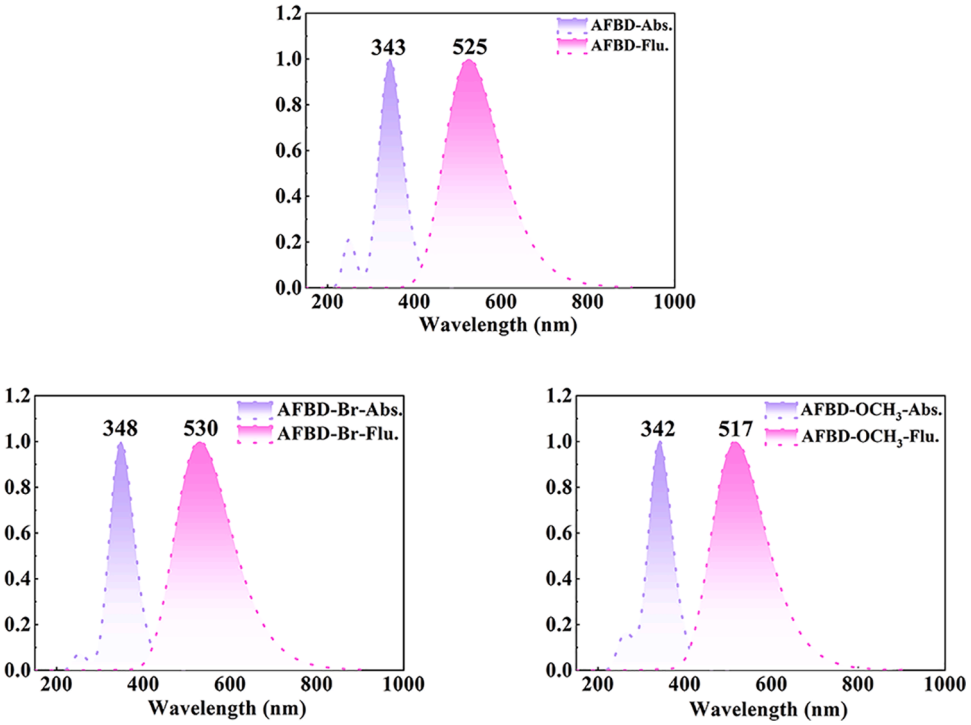

Fig. 3. The normalized absorption and fluorescence spectra of AFBD, AFBD-Br and AFBD–OCH_3 in acetonitrile solvent.

Table 3
The absorption characteristics of AFBD, AFBD-Br and AFBD–OCH_3 in acetonitrile solvent at the theoretical level of TDDFT/B3PW91/6–31++G. (H and L represent HOMO and LUMO, respectively).

	State	E_{abs} (eV)	λ_{abs} (nm)	F	Contribution	CI (%)
AFBD	S_1	3.610eV	343	0.4416	H→L	69.93%
	S_2	4.265eV	291	0.0014	H-2→L	70.44%
	S_5	4.970eV	249	0.0929	H→L + 2	64.42%
AFBD-Br	S_1	3.562eV	348	0.4805	H→L	69.91%
	S_2	4.248eV	292	0.0011	H-2→L	70.40%
	S_3	4.462eV	278	0.0049	H-1→L	64.72%
	S_4	4.595eV	270	0.0002	H→L + 1	64.27%
	S_6	4.922eV	252	0.0336	H→L + 2	55.76%
AFBD–OCH_3	S_1	3.628eV	342	0.4363	H→L	69.82%
	S_2	4.377eV	283	0.0010	H-2→L	70.41%
	S_3	4.451eV	279	0.0242	H-1→L	66.15%
	S_4	4.917eV	267	0.0288	H→L + 1	66.12%
	S_5	4.917eV	252	0.0343	H→L + 2	57.36%
	S_6	5.322eV	233	0.0001	H-5→L	53.12%

AFBD–OCH_3, representing the IHBs of O_1-H_1... N_1 and O_2-H_2...N_2. Here, for O_1-H_1...N_1 and O_2-H_2...N_2, the strength of IHBs in different electronic groups follows the order of Br>OCH_3>H and OCH_3>H>Br, respectively. This result is consistent with the structural analysis. For the S_1 state, the two spike peaks of three compounds are located in the vicinity of −0.04 ~ −0.05, which are attributed to the two new IHBs O_1...H_1-N_1 and O_2...H_2-N_2. During the process from S_0 to S_1 state, the IHBs undergo a change, where the protons H_1 and H_2 transfer to the N_1 and N_2 atoms. Therefore, the above results confirm the occurrence of ESIDPT in the S_1 state.

3.3. Infrared (IR) spectra

The IR spectra is considered an effective tool to evaluate the ESPT process [45,46]. In order to prove the point put forward in the previous section again: "The ESIDPT process happen in the S_1 state". We simulate the IR spectra (scale factor 0.972) of AFBD, AFBD-Br and AFBD–OCH_3. The calculated vibration frequency scopes from 2100cm^{-1} to 3600cm^{-1}, including only the vibration peaks of O_1-H_1, O_2-H_2 and N_1-H_1, N_2-H_2 groups associated with the IHBs.

As shown in Fig. 2, due to the symmetric structure of AFBD, there is only a vibration peak near 2413cm^{-1} in the S_0 state and 3178cm^{-1} in the S_1 state, which is attributed to O_1-H_1&O_2-H_2 and N_1-H_1&N_2-H_2 stretching vibration respectively. For the AFBD-Br and AFBD–OCH_3, the O_1-H_1 and O_2-H_2 vibration peaks are 2106 cm^{-1}, 2283 cm^{-1} and 2501 cm^{-1}, 2319 cm^{-1} in the S_0 state. When excited to the S_1 state, the N_1-H_1 and N_2-H_2 vibration peaks are separately located at 3199 cm^{-1}, 3232 cm^{-1} and 3176cm^{-1}, 3160cm^{-1}. Interestingly, it can be seen that from the S_0 state to the S_1 state, the original O_1-H_1 and O_2-H_2 vibration peaks disappear in three compounds, while the new N_1-H_1 and N_2-H_2 vibrational peaks form. It indicates that the proton H_1 and H_2 are transferred from proton donors O_1 and O_2 to proton receptors N_1 and N_2, realizing the ESIDPT process.

3.4. Electronic spectra and frontier molecular orbitals (FMOs)

For to get to know the effect of different electronic groups on the photophysical properties in target molecule, Fig. 3 has shown the electronic spectra of AFBD, AFBD-Br and AFBD–OCH_3 in acetonitrile solvent at the level of TD-DFT/B3PW91/6–31++G. Their absorption characteristics in the first six singlet excited states are gathered in Table 3, including the lowest vertical excitation energies (E_{abs}), absorption peaks (λ_{abs}), corresponding oscillator strengths (f>0) and orbital transition contributions. In addition, based on the optimized S_1 configuration of AFBD and its two derivatives in acetonitrile solvent, we calculate and draw the corresponding fluorescence spectra in Fig. 3.

As noted in Fig. 3, the theoretical absorption and fluorescence peaks of AFBD in acetonitrile solvent are at 343 nm and 525 nm respectively, which are consistent with the experimental data of 345 nm and 506 nm [29]. It suggests that the selected functional is dependable. Moreover, the absorption and fluorescence peaks of AFBD-Br and AFBD–OCH_3 separately are 348 nm, 342 nm and 530 nm, 517 nm. It is worth mentioning that the Stoke shifts are generated by keto form in AFBD, AFBD-Br and AFBD–OCH_3 are 182 nm, 182 nm and 175 nm. The above finds indicate that the three compounds are endowed with excellent optical behaviors due to the large Stokes shift, which make them have a potential application prospect in many cutting-edge fields.

Subsequently, in order to exhibit the transition contribution from the ground state to each electron excited state, we calculate the contribution of each transition with oscillation strength (f) greater than 0.02 in three compounds and plot them into the refined absorption spectra in Fig. S2.

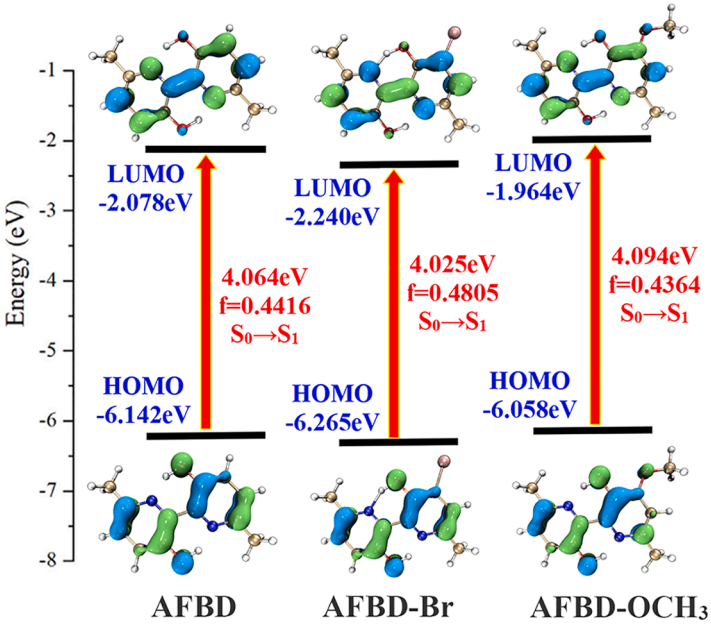

Fig. 4. The frontier molecular orbitals (FMOs) and HOMO→LUMO energy gaps of AFBD, AFBD-Br, and AFBD–OCH_3 in acetonitrile solvent.

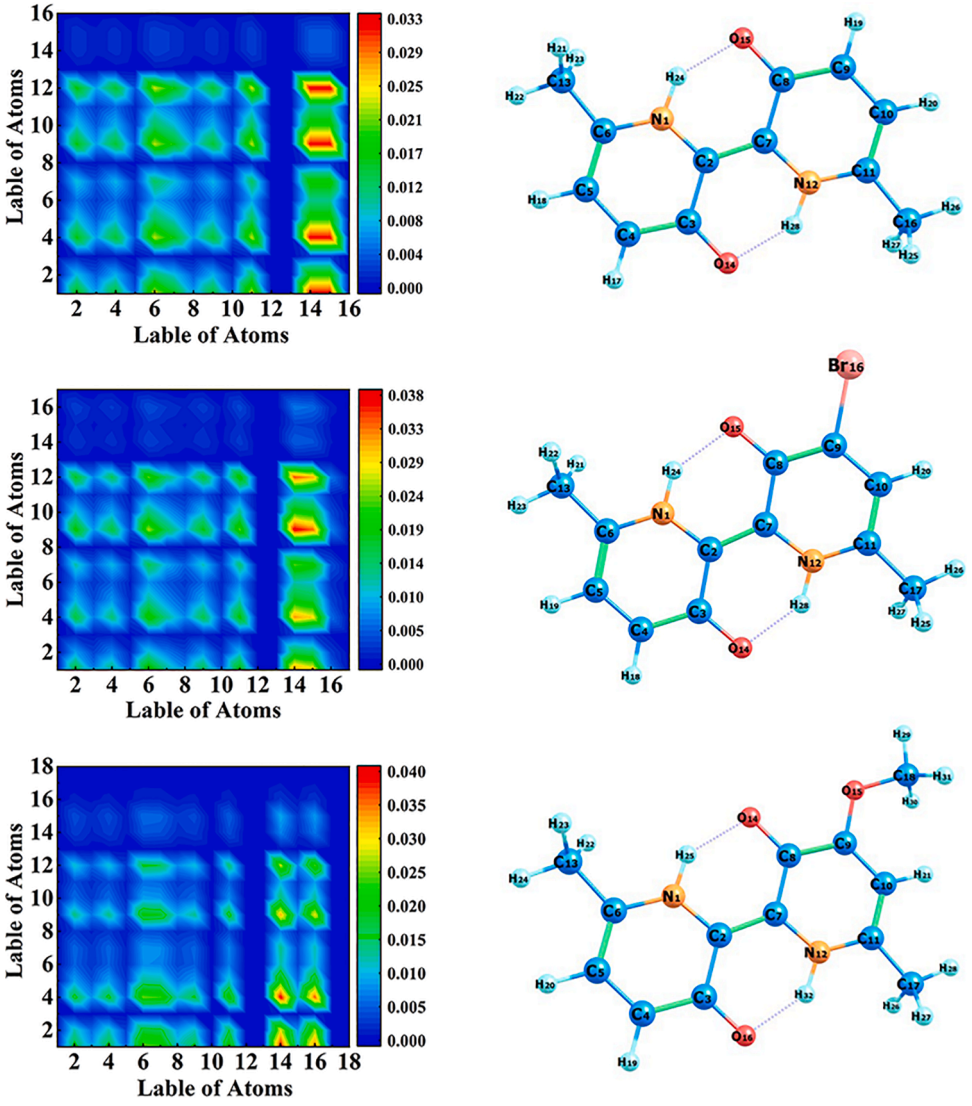

Fig. 5. The transition density matrix (TDM) and atomic numbers diagrams of AFBD (up), AFBD-Br (middle) and AFBD–OCH_3 (down) in acetonitrile solvent.

Among them, the horizontal position of the black vertical lines is the absorption wavelength, and the height of the vertical lines is the oscillator strength (corresponding to the right axis). Significantly, the dual absorption peaks have emerged, and the lower intensity principally stems from the transition $S_0 \rightarrow S_5$ of AFBD, AFBD–OCH_3 and $S_0 \rightarrow S_6$ of AFBD-Br. According to expectation, their maximum absorption peaks completely spring from the first singlet state transition ($S_0 \rightarrow S_1$), which is dominantly related to the HOMO→LUMO transition (see Table 3). It follows that only the HOMO and LUMO in three compounds are displayed in Fig. 4. As shown in the FMOs diagram, the substitution of electronic groups OCH_3→H→Br makes the HOMO→LUMO energy gaps gradually narrow, thereby resulting in the red-shift of the absorption peak from AFBD–OCH_3 (342 nm) to AFBD (343 nm) and AFBD-Br (348 nm). Additionally, the HOMO→LUMO transition exhibits π-π* type feature, which plays an important role in facilitating the excited state proton transfer behavior. We also notice that the electron density distribution moves from the proton donors (O_1 and O_2) to the proton acceptors (N_1 and N_2), which make the acidity and basicity of the proton donor and acceptor parts stronger and further promoting the progress of the ESIDPT.

In addition to these, we also refer to the atomic numbers of AFBD, AFBD-Br and AFBD–OCH_3 to analyze their transition density matrix (TDM) diagrams. As illustrated in Fig. 5, it can be seen that the charge

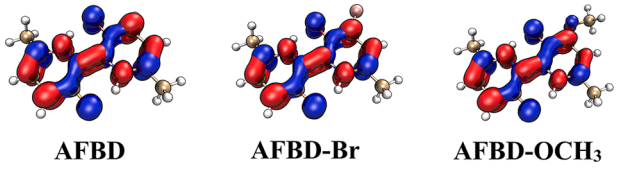

Fig. 6. Calculated the charge density difference (CDD) maps related to the $S_0 \rightarrow S_1$ transition.

density of atoms No. 4 and No. 9 in the diagonal matrix has significantly changed after photoexcitation. At the same time, we find that two hydroxy oxygens (No.14 and No.15) show strong electron-hole correlation with N_2 atom (No.12), C atom (No.9) and N_1 atom (No.1), C atom (No.4) respectively via analyzing the off-diagonal elements. The correlation of these regions implies that the charge population has obvious differences before and after the electronic transition. That is, the intramolecular charge transfer (ICT) process can occur in the electronic excited state.

To more intuitively study the change in electron density during the process of light excitation, the CDD maps of AFBD, AFBD-Br and AFBD–OCH_3 from the S_0 state to the S_1 state are visualized in Fig. 6. The red and blue separately indicate the regions with increasing and decreasing charge density. Apparently, the net electron density of the

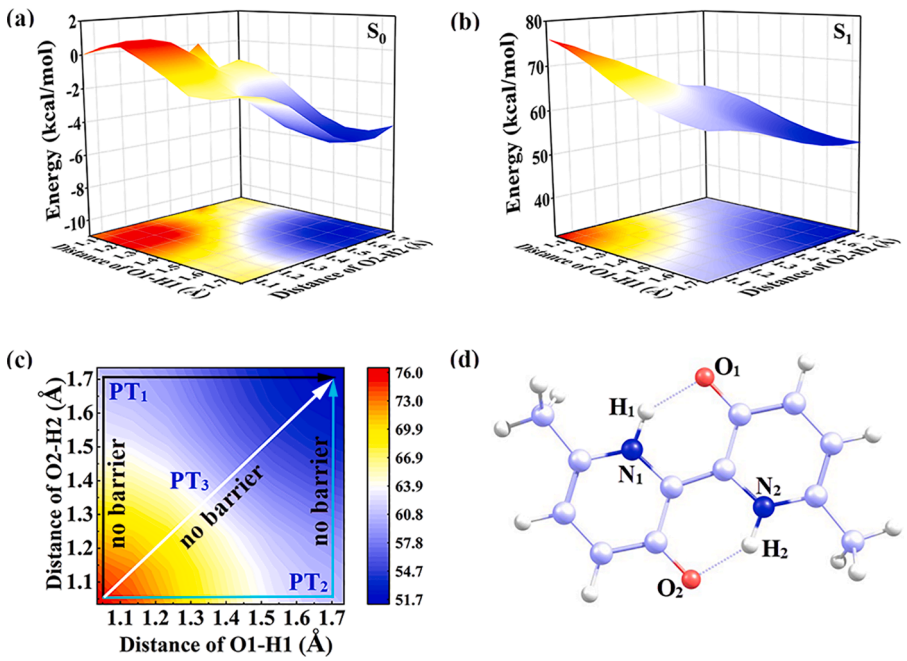

Fig. 7. The S_0- (a) and S_1-stated (b) PES for AFBD in acetonitrile solvent. (c) Top view of the S_1 stated PES. (d) The geometry of AFBD in the S_1 state.

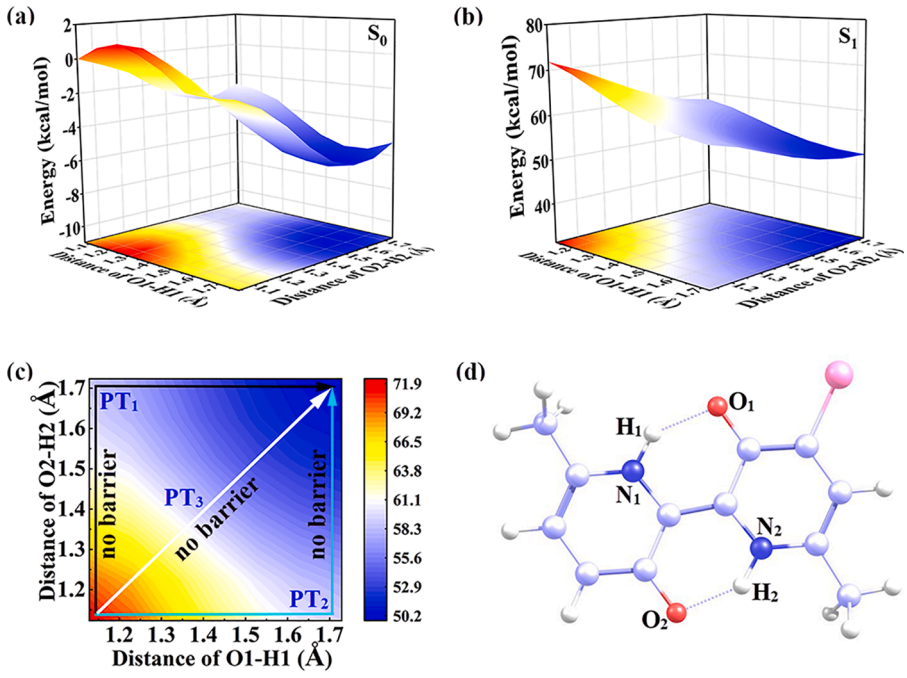

Fig. 8. The S_0- (a) and S_1-stated (b) PES for AFBD-Br in acetonitrile solvent. (c) Top view of the S_1 stated PES. (d) The geometry of AFBD-Br in the S_1 state.

two hydroxyl oxygens (O_1 and O_2) related to the ESIDPT process decreases, while that of the proton receptors (N_1 and N_2) increases. This remarkable ICT explains that the electronegativities of nitrogen atoms in the S_1 state is stronger than that of oxygen atoms. Therefore, the CDD analysis indicates that the ability of two nitrogen atoms (N_1 and N_2) to attract the protons (H_1 and H_2) is strengthened, which in turn accelerates the occurrence of ESIDPT process.

3.5. Potential energy surface (PES)

Owing to the presence of dual IHBs in AFBD, AFBD-Br and AFBD–OCH_3, the pathway experienced by the ESIDPT process is an important point worth pondering and discussing. Therefore, for the sake of addressing this issue and concurrently providing precise energy barriers required for proton transfer process. We scan the 3D potential energy surface in the S_0 and S_1 states of AFBD (in Fig. 7), AFBD-Br (in Fig. 8) and AFBD–OCH_3 (in Fig. 9) along the possible photochemical reaction pathways by fixing O_1—H_2 and O_2—H_2 bond length from 1.0 Å to 1.8 Å in the step of 0.1 Å. And the top view of the S_0 stated PES is detailed in Fig. S3. In addition, the possible proton transfer pathways have been marked on PES and can be divided into three types (PT_1 and PT_2 are defined as stepwise mechanism, PT_3 is a cooperative mechanism): (1) PT_1→proton H_1 first moves from O_1 to N_1, and then proton H_2 moves from O_2 to N_2. (2) PT_2→The situation is exactly opposite to PT_1.

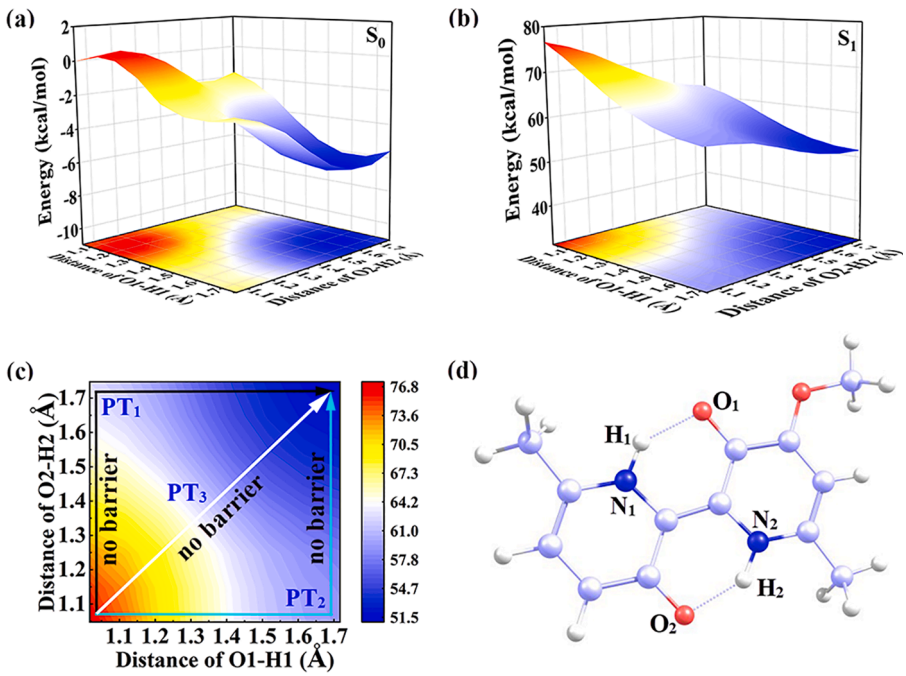

Fig. 9. The S_0- (a) and S_1-stated (b) PES for AFBD–OCH_3 in acetonitrile solvent. (c) Top view of the S_1 stated PES. (d) The geometry of AFBD–OCH_3 in the S_1 state.

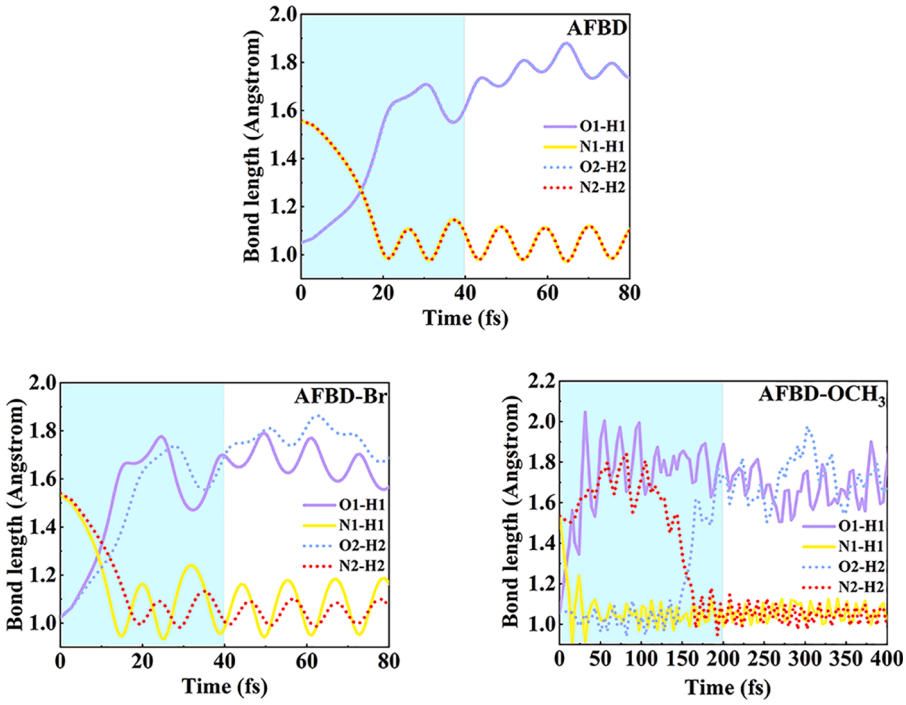

Fig. 10. The important bond length distances with time evolution for AFBD, AFBD-Br and AFBD–OCH_3 in the S_1 state.

(3) PT_3→The two protons (H_1 and H_2) move simultaneously from O_1 and O_2 to N_1 and N_2, respectively.

In the S_0 state, the three different proton transfer pathways of AFBD and its two derivatives require overcoming about 0.37–1.14 kcal/mol energy barrier. It is noteworthy that, under excitation of light, the energy barriers of PT1, PT2 and PT3 in three compounds are all barrier free. These discussions indicate that the double proton transfer process in three compounds is more likely to occur in the S_1 state than in the S_0 state. However, it is not yet clear whether their ESIDPT process is a cooperative or stepwise mechanism.

3.6. *Excited state hydrogen bonding dynamics*

To further clarify the detailed excited state proton transfer mechanism and find out whether the stepwise ESIDPT or cooperative ESIDPT occur for three compounds. We theoretically present the time scale and characteristic of the ESIDPT process in AFBD, AFBD-Br and AFBD–OCH_3 at the fs level and further unveil via the excited state hydrogen bonding dynamics in Fig. 10 [47–50].

At the beginning of the simulation, the bond lengths O_1-H_1 and O_2-H_2 of AFBD gradually increase with extension of time, while those of N_1-H_1

and N_2-H_2 gradually decrease with extension of time. This indicates that protons H_1 and H_2 rapidly move from O_1 and O_2 to N_1 and N_2 along intramolecular hydrogen bondings until protons H_1 and H_2 are transferred. In other words, the distance between O_1-H_1&N_1-H_1 intersect with O_2-H_2&N_2-H_2 at ~15 fs. Combined with the potential energy surface analysis, AFBD occurs the cooperative (PT_3) ESIDPT process at ~15 fs in the S_1 state.

When AFBD is substituted by electron-withdrawing (-Br) and electron-donating (–OCH_3) groups, the path and time scale of the ESIDPT process are different due to the influence of charge distribution after photoexcitation. For AFBD-Br, the entire event occurs at ~12 fs. First, the O_1-H_1 bond disrupts and the new N_1-H_1 bond borns at ~9 fs, then the O_2-H_2 bond disrupts and the new N_2-H_2 bond borns at ~12 fs, completing the stepwise (PT_1→PT_2) ESIDPT process. In AFBD–OCH_3, we do not observe the intersection of O_2-H_2 and N_2-H_2 within the maximum simulation time of 80 fs. Therefore, we expand the time step and set the simulation time to 400 fs. According to the breaking of O_1-H_1&O_2-H_2 and the formation of N_1-H_1&N_2-H_2, the whole stepwise (PT_1→PT_2) ESIDPT process has completed at ~155 fs. These results confirm that the substitution of the electronic groups OCH_3→H→Br can accelerate the ESIDPT process.

4. Conclusion

In this research, the influence of different electronic groups on the photophysical properties in AFBD and its two derivatives has been systematically investigated by the DFT and TD-DFT methods. The existence of the ESIDPT process in three compounds is proved by acquired geometric parameters, RDG scatter plots, and IR spectra data. From the FMOs and CDD maps, the obvious ICT features after light excitation can promote the ESIDPT process. Based on the scanned 3D potential energy surface, it could be found that the ESIDPT process is more inclined to happen in the S_1 state. Moreover, we also evaluate the time scale and characteristic of the ESIDPT process through excited state hydrogen bonding dynamics and confirm that AFBD experience a cooperative ESIDPT process at ~15 fs. More importantly, the cooperative ESIDPT is converted into the stepwise ESIDPT under the entry of the electron-withdrawing (-Br) and the electron-donating (–OCH_3) groups. Besides, the entire stepwise ESIDPT in AFBD-Br and AFBD–OCH_3 occurs at ~12 fs and ~155 fs respectively. In a conclusion, the substitution of the electronic groups OCH_3→H→Br not only changes the internal mechanism, but also facilitates the ESIDPT process.

CRediT authorship contribution statement

Hongyan Mu: Writing – original draft, Data curation, Conceptualization, Writing – review & editing. **Dan Li:** Data curation, Writing – original draft. **Jiaan Gao:** Methodology. **Yang Wang:** Investigation. **Yifu Zhang:** Software. **Guangyong Jin:** Resources, Supervision. **Hui Li:** Writing – review & editing, Conceptualization, Funding acquisition.

Declaration of Competing Interest

The authors declare that they have no known competing financial interests or personal relationships that could have appeared to influence the work reported in this paper.

Data availability

No data was used for the research described in the article.

Acknowledgments

This work was supported financially by the Science and Technology Department of Jilin Province (YDZJ202101ZYTS043) and the National Natural Science Foundation of China (No.12004051).

Supplementary materials

Supplementary material associated with this article can be found, in the online version, at doi:10.1016/j.molstruc.2023.136385.

References

[1] C.C. Hsieh, C.M. Jiang, P.T. Chou, Recent experimental advances on excited-state intramolecular proton coupled electron transfer reaction, Acc. Chem. Res. 43 (2010) 1364–1374, https://doi.org/10.1021/ar1000499.
[2] G.J. Zhao, K.L. Han, Hydrogen bonding in the electronic excited state, Acc. Chem. Res. 45 (2012) 404–413, https://doi.org/10.1021/ar200135h.
[3] G.L. Cui, Z.G. Lan, W. Thiel, Intramolecular hydrogen bonding plays a crucial role in the photophysics and photochemistry of the GFP chromophore, J. Am. Chem. Soc. 134 (2012) 1662–1672, https://doi.org/10.1021/ja208496s.
[4] A. Jezierska, B. Kiziora, B.M. Szyja, J.J. Panek, On the nature of inter- and intramolecular interactions involving benzo[h]quinoline and 10-hydroxybenzo[h] quinoline: electronic ground state vs excited state study, J. Mol. Struct. 1234 (2021), 130126, https://doi.org/10.1016/j.molstruc.2021.130126.
[5] C.X. Yao, Y.Q. Zhong, Y.R. Guo, New insights into the excited state of an A-D-A quadrupolar molecule strongly hydrogen bonded to molecules of methanol and hexafluoro isopropanol, J. Mol. Struct. 1273 (2023), 134294, https://doi.org/10.1016/j.molstruc.2022.134294.
[6] Z.L. Ding, S.J. Ji, J.F. Zhao, D.Y. Zheng, Combination of theoretical calculation and experiment to study the excited state proton transfer behavior of trifluoroacetamidoanthraquinone with different substitution positions, J. Mol. Struct. 1252 (2022), 132084, https://doi.org/10.1016/j.molstruc.2021.132084.
[7] H.Y. Mu, Y.H. Sun, J.A. Gao, C. Xin, H.F. Zhao, G.Y. Jin, H. Li, Switching the ESIPT and TICT process of DP-HPPI via intermolecular hydrogen bonding, J. Mol. Struct. 1277 (2023), 134800, https://doi.org/10.1016/j.molstruc.2022.134800.
[8] L.C. Sun, Y.C. Chen, M.T. Sun, Exploring nonemissive excited-state intramolecular proton transfer by plasmon-enhanced hyper-raman scattering and two-photon excitation fluorescence, J. Phys. Chem. C 126 (2022) 487–492, https://doi.org/10.1021/acs.jpcc.1c10041.
[9] H.Y. Mu, H. Li, C.F. Sun, J.A. Gao, M. Yang, C. Xin, G.Y. Jin, Different competition mechanism between ESPT and TICT process regulated by protic and aprotic solvent in DHP, J. Mol. Liq. 375 (2023), 121278, https://doi.org/10.1016/j.molliq.2023.121278.
[10] V.S. Padalkar, S. Seki, Excited-state intramolecular proton-transfer (ESIPT) inspired solid state emitters, Chem. Soc. Rev. 45 (2016) 169–202, https://doi.org/10.1039/C5CS00543D.
[11] A.C. Sedgwick, L.L. Wu, H.H. Han, S.D. Bull, X.P. He, T.D. James, J.L. Sessler, B. Z. Tang, H. Tian, J. Yoon, Excited-state intramolecular proton-transfer (ESIPT) based fluorescence sensors and imaging agents, Chem. Soc. Rev. 47 (2018) 8842–8880, https://doi.org/10.1039/C8CS00185E.
[12] X.F. Yang, Q. Huang, Y.G. Zhong, Z. Li, H. Li, M. Lowry, J.O. Escobedo, R. M. Strongin, A dual emissionfluorescent probe enables simultaneous detection of glutathione and cysteine/homocysteine, Chem. Sci. 5 (2014) 2177–2183, https://doi.org/10.1039/C4SC00308J.
[13] T. Mutai, H. Tomoda, T. Ohkawa, Y. Yabe, K. Araki, Switching of polymorph-dependent ESIPT luminescence of an imidazo [1,2-a] pyridine derivative, Angew. Chem. Int. Edit. 47 (2008) 9664–9666, https://doi.org/10.1002/ange.200803975.
[14] L.J. Tang, X. Dai, K.L. Zhong, D. Wu, X. Wen, A novel 2,5-diphenyl-1,3,4-oxadiazole derived fluorescent sensor for highly selective and ratiometric recognition of Zn^{2+} in water through switching on ESIPT, Sensor Actuat. B-Chem. 203 (2014) 557–564, https://doi.org/10.1016/j.snb.2014.07.022.
[15] J.E. Kwon, S.Y. Park, Advanced Organic Optoelectronic Materials: harnessing Excited-State Intramolecular Proton Transfer (ESIPT) Process, Adv. Mater. 23 (2011) 3615–3642, https://doi.org/10.1002/adma.201102046.
[16] J.Z. Zhao, S.M. Ji, Y.H. Chen, H.M. Guo, P. Yang, Excited state intramolecular proton transfer (ESIPT): from principal photophysics to the development of new chromophores and applications influorescent molecular probes and luminescent materials, Phys. Chem. Chem. Phys. 14 (2012) 8803–8817, https://doi.org/10.1039/C2CP23144A.
[17] S. Mukherjee, P. Thilagar, Organic white-light emitting materials, Dyes. Pigment. 110 (2014) 2–27, https://doi.org/10.1016/j.dyepig.2014.05.031.
[18] P. Chou, D. McMorrow, T. Aartsma, M. Kasha, The proton-transfer laser. Gain spectrum and amplification of spontaneous emission of 3-hydroxyflavone, J. Phys. Chem. 88 (1984) 4596–4599, https://doi.org/10.1021/j150664a032.
[19] C.Z. Li, D.L. Li, Chi. Ma, Y.F. Liu, DFT-TDDFT investigation of excited-state intramolecular proton transfer in 2- (2′-hydroxyphenyl)benz- imidazole derivatives: effects of electron acceptor and donor groups, J. Mol. Liq. 224 (2016) 83–88, https://doi.org/10.1016/j.molliq.2016.09.088.
[20] D.P. Yang, W.P. Yang, Y.S. Tian, R. Zheng, Regulating the excited state behaviors of 2-benzooxazol-2-yl-4,6-di-tert-butyl-phenol fluorophore by solvent polarity: a theoretical simulation, Chem. Phys. 558 (2022), 111513, https://doi.org/10.1016/j.chemphys.2022.111513.
[21] C.J. Shang, Y.J. Cao, C.F. Sun, Y.Z. Li, Unveiling the influence of atomic electronegativity on the double ESIPT processes of uralenol: a theoretical study, Spectrochim. Acta. A 268 (2022), 120660, https://doi.org/10.1016/j.saa.2021.120660.

[22] J.F. Zhao, H.H. Zhang, L.M. Fan, F.Y. Li, P. Song, Unveiling and regulating the solvent-polarity-associated excited state intramolecular double proton transfer behavior for 1-bis(benzothiazolyl)naphthalene-diol fluorophore, J. Lumin. 299 (2023), 122831, https://doi.org/10.1016/j.saa.2023.122831.
[23] A. Kundu, S. Karthikeyan, D. Moon, S.P. Anthony, Excited state intramolecular proton transfer induced fluorescence in triphenylamine molecule: role of structural conformation and reversible mechanofluorochromism, J. Mol. Struct. 1169 (2018) 1–8, https://doi.org/10.1016/j.molstruc.2018.05.042.
[24] C. Ning, C.Y. Xiao, R.F. Lu, P.W. Zhou, Whether the excited state intramolecular proton transfer of 1-hydroxy-2-acetonaphthone will happen? J. Lumin. 217 (2020), 116825 https://doi.org/10.1016/j.jlumin.2019.116825.
[25] J.F. Zhao, B. Jin, Solvent polarity dependent excited state hydrogen bond effects and intramolecular double proton transfer mechanism for 2-hydroxyphenyl-substituted benzo [1,2-d:4,5-d'] bisimidazole system, Spectrochim. Acta. A 250 (2021), 119394, https://doi.org/10.1016/j.saa.2020.119394.
[26] X.F. Yu, S. Yamazaki, T. Taketsugu, Solvent effects on the excited-state double proton transfer mechanism in the 7-azaindole dimer: a TDDFT study with the polarizable continuum model, Phys. Chem. Chem. Phys. 19 (2017) 23289–23301, https://doi.org/10.1039/C7CP04942K.
[27] L.F. Xu, Q. Wang, Y.R. Zhang, Electronic effect on the photophysical properties of 2-(2-hydroxyphenyl)benzothiazole-based excited state intramolecular proton transfer fluorophores synthesized by sonogashira-coupling reaction, Dyes Pigment. 136 (2017) 732–741, https://doi.org/10.1016/j.dyepig.2016.09.024.
[28] C. Hansch, A. Leo, R.W. Taft, A survey of Hammett substituent constants and resonance and field parameters, Chem. Rev. 91 (1991) 165–195, https://doi.org/10.1021/cr00002a004.
[29] G. Ulrich, F. Nastasi, P. Retailleau, F. Puntoriero, R. Ziessel, S. Campagna, Luminescent excited-state intramolecular proton-transfer (ESIPT) dyes based on 4-Alkyne-Functionalized[2,2′-B*ipyridine*]-3,3′-ᴅ- iol, Dyes 14 (2008) 4381–4392, https://doi.org/10.1002/chem.200701803.
[30] M.J. Frisch, G.W. Trucks, H.B. Schlegel, G.E. Scuseria, M.A. Robb, J.R. Cheeseman, G. Scalmani, V. Barone, B. Mennucci, G.A. Petersson, H. Nakatsuji, M. Caricato, X. Li, H.P. Hratchian, A.F. Izmaylov, J. Bloino, G. Zheng, J.L. Sonnenberg, M. Hada, M. Ehara, K. Toyota, R. Fukuda, J. Hasegawa, M. Ishida, T. Nakajima, Y. Honda, O. Kitao, H. Nakai, T. Vreven, J.A. Montgomery Jr., J.E. Peralta, F. Ogliaro, M. J. Bearpark, J. Heyd, E.N. Brothers, K.N. Kudin, V.N. Staroverov, R. Kobayashi, J. Normand, K. Raghavachari, A.P. Rendell, J.C. Burant, S.S. Iyengar, J. Tomasi, M. Cossi, N. Rega, N.J. Millam, M. Klene, J.E. Knox, J.B. Cross, V. Bakken, C. Adamo, J. Jaramillo, R. Gomperts, R.E. Stratmann, O. Yazyev, A.J. Austin, R. Cammi, C. Pomelli, J.W. Ochterski, R.L. Martin, K. Morokuma, V.G. Zakrzewski, G.A. Voth, P. Salvador, J.J. Dannenberg, S. Dapprich, A.D. Daniels, Ö. Farkas, J. B. Foresman, J.V. Ortiz, J. Cioslowski, D.J. Fox, Gaussian 09, Gaussian, Inc., Wallingford, CT, USA, 2009.
[31] M. Oftadeh, Z. Barfarakh, F. Ravari, Luminescent excited-state intramolecular proton-transfer dyes based on 4-functionalized 6, 6′ -dimethyl-3, 3′ -dihydroxy-2, 2′-bipyridine (BP(OH)2-Rs); DFT simulati- on study, J. Mol. Graph. Model. 107 (2021), 107948, https://doi.org/10.1016/j.jmgm.2021.107948.
[32] I.M. Alecu, J.J. Zheng, Y. Zhao, D.G. Truhlar, Computational thermochemistry: scale factor databases and scale factors for vibrational frequencies obtained from electronic model chemistries, J. Chem. Theory. Comput. 6 (2010) 2872–2887, https://doi.org/10.1021/ct100326h.
[33] B.F. Cao, Y. Li, Q. Zhou, B. Li, X. Su, H. Yin, Y. Shi, Synergistically improving myricetin ESIPT and antioxidant activity via dexterously trimming atomic electronegativity, J. Mol. Liq. 325 (2021), 115272, https://doi.org/10.1016/j.molliq.2020.115272.
[34] X. Xin, W. Shi, Y. Zhao, G.J. Zhao, Y.Q. Li, Theoretical insights into the excited-state single and double proton transfer processes of DEASH in water, 570 (2023) 111882. https://doi.org/10.1016/j.chemphys.2023.111882.
[35] E. Cances, B. Mennucci, J. Tomasi, A new integral equation formalism for the polarizable continuum model: theoretical background and applications to isotropic and anisotropic dielectrics, J. Chem. Phys. 107 (1997) 3032–3041, https://doi.org/10.1063/1.474659.
[36] R. Cammi, J. Tomasi, Remarks on the use of the apparent surface charges (ASC) methods in solvation problems: iterative versus matrix-inversion procedures and the renormalization of the apparent charges, J. Comput. Chem. 16 (1995) 1449–1458, https://doi.org/10.1002/jcc.540161202.
[37] B. Mennucci, E. Cances, J. Tomasi, Evaluation of solvent effects in isotropic and anisotropic dielectrics and in ionic solutions with a unified integral equation method: theoretical bases, computational implementation, and numerical applications, J. Phys. Chem. B 101 (1997) 10506–10517, https://doi.org/10.1021/jp971959k.
[38] P.D. Nguyen, F.Z. Ding, S.A. Fischer, W. Liang, X.S. Li, Solvated first-principles excited-state charge-transfer dynamics with time-depende-nt polarizable continuum model and solvent dielectric relaxation, J. Phys. Chem. Lett. 3 (2012) 2898–2904, https://doi.org/10.1021/jz301042f.
[39] A. Petrone, D.B. Lingerfelt, D.B. Williams-Young, X.S. Li, Ab initio transient vibrational spectral analysis, J. Phys. Chem. Lett. 7 (2016) 4501–4508, https://doi.org/10.1021/acs.jpclett.6b02292.
[40] T.F. Stetina, S.C. Sun, D.B. Lingerfelt, A. Clark, X.S. Li, The role of excited-state proton relays in the photochemical dynamics of water nanodroplets, J. Phys. Chem. Lett. 10 (2019) 3694–3698, https://doi.org/10.1021/acs.jpclett.9b01062.
[41] T. Lu, F.W. Chen, Multiwfn: a multifunctional wavefunction analyzer, J. Comput. Chem. 33 (2012) 580–592, https://doi.org/10.1002/jcc.22885.
[42] W. Humphrey, A. Dalke, K. Schulten, VMD: visual molecular dynamics, J. Mol. Graph. 14 (1996) 33–38, https://doi.org/10.1016/0263-7855(96)00018-5.
[43] E.R. Johnson, S. Keinan, P. Mori-Sanchez, J.L. Contreras-Garcia, A.J. Cohen, W. T. Yang, Revealing noncovalent interactions, J. Am. Chem. Soc. 132 (2010) 6498–6506, https://doi.org/10.1021/ja100936w.
[44] T. Lu, Q. Chen, Interaction region indicator: a simple real space function clearly revealing both chemical bonds and weak interactions, Chem.-Method. 1 (2021) 231–239, https://doi.org/10.1002/cmtd.202100007.
[45] G.J. Zhao, K.L. Han, Time-dependent density functional theory study on hydrogen-bonded intramolecular charge-transfer excited state of 4-dimethylamino-benzonitrile in methanol, J. Comput. Chem. 29 (2008) 2010–2017, https://doi.org/10.1002/jcc.20957.
[46] F.B. Yu, P. Li, B.S. Wang, K.L. Han, Reversible near-Infrared fluorescent probe introducing tellurium to mimetic glutathione peroxidase for monitoring the redox cycles between peroxynitrite and glutathione in vivo, J. Am. Chem. Soc. 135 (2013) 7674–7680, https://doi.org/10.1021/ja401360a.
[47] M. Dommett, R. Crespo-Otero, Excited state proton transfer in 2'-hydroxychalcone derivatives, Phys. Chem. Chem. Phys. 19 (2017) 2409–2416, https://doi.org/10.1039/C6CP07541J.
[48] J.F. Zhao, Z.J. Li, B. Jin, Uncovering photo-induced hydrogen bonding interaction and proton transfer mechanism for the novel salicylaldehyde azine derivative with para-position electrophilic cyano group, J. Lumin. 238 (2021), 118231, https://doi.org/10.1016/j.jlumin.2021.118231.
[49] H. Yin, B. Li, X. Zhao, Y.L. Liu, Y. Shi, D.J. Ding, Restriction of intramolecular torsion induces abnormal blue-shifted fluorescence in the aggregate state, Dye. Pigment. 201 (2022), 110192, https://doi.org/10.1016/j.dyepig.2022.110192.
[50] H.W. Zhang, Z.X. Li, J.R. Liu, Y. Wang, Effect of intermolecular hydrogen bonds on the proton transfer and fluorescence characteristics of 10-hydroxy-20-acetonaphthone, J. Mol. Liq. 361 (2022), 119555, https://doi.org/10.1016/j.molliq.2022.119555.